Vision, Modeling, and Visualization (2014)
J. Bender, A. Kuijper, T. von Landesberger, H. Theisel and P. Urban (Eds.)

Curvature-Based Crease Surfaces for Wave Visualization

G. Aldrich[1,3], A. Gimenez[1], M. Oskin[2], R. Strelitz[3], J. Woodring[3], L. H. Kellogg[2] and B. Hamann[1]

[1]Department of Computer Science, University of California, Davis, California USA
[2]Department of Geology, University of California, Davis, California USA
[3]CCS Division, Los Alamos National Laboratory, New Mexico USA

Abstract

The visualization and analysis of complex fields often requires identifying and extracting domain specific features. Through a collaboration with geophysicists we extend previous work on crease surfaces with a new and complimentary definition: extremas in principal surface curvature rather than scalar value. Using this definition, we visualize the resulting surfaces which correspond to individual wave fronts. As these wave fronts propagate through a control structure (medium), they undergo changes in intensity, shape and topology due to reflection, refraction and interference. We demonstrate our ability to effectively visualize these phenomena in complex data sets including a large-scale simulation of a hypothetical earthquake along the San Andreas fault in Southern California.

Categories and Subject Descriptors (according to ACM CCS): I.3.7 [Computer Graphics]: Visible line/surface algorithms—

1. Introduction

Visualizing wave phenomena over a three-dimensional (3D) spatial domain is a difficult problem due to the volatile and unpredictable nature of wave fields. As individual wave fronts propagate, they reflect off material boundaries, refract as the density of the materials change, and cause interference as wave fronts combine. The intensity, shape and topology of wave fronts also change as they interact with the medium. These aspects are key to understanding a wave's motion through time, as well as the importance and accuracy of material boundaries used as part of a numerical simulation. Unfortunately classic visualization methods are not wholly adequate for visualizing some of the most important wave characteristics: volume rendering occludes important details; iso-surface rendering is not representative of the wave's structure; slicing is classically the best tool and shows all the details in a plane, but it is incapable of showing changes over the 3D spatial domain. Therefore, we investigated ways of automatically segmenting the wave field into a set of features that are meaningful to domain scientists, and intuitively describe the shape and topology of the volumetric wave field as a whole.

When asked to think of a wave's motion over time, the image that most often comes to mind is that of ripples in a pond or ocean swells breaking on a beach. Surface waves, by their very nature, are easier to understand because we have so many physical examples which are readily apparent in everyday life. It is common practice, when visualizing waves over a 3D domain, to slice the data and then transform that slice into a height map of wave intensity, Fig. 8, effectively emulating a surface wave on the plane. Using such an approach, the viewer can intuitively understand and relate to the interactions that occur as the wave propagates and changes. However, by limiting the visualization and analysis to a few representative planes, much of the volumetric information is lost.

We represent the form of a wave field defined over a 3D domain using fiduciary objects, features in the physical 3D domain that are representative of the wave as a whole. Our chosen objects are surfaces representing those areas in the volume where the wave's associated energy function is changing most abruptly. For a function representing propagating waves, we consider crease surface behavior that correspond directly to individual wave fronts whose intensity can be rendered using color, opacity or a combination. By using these fiduciary objects, we generate an intuitively understandable representation that is conceptually similar to a deformed slice through the volume. These surfaces can be used to better understand structural changes in the wave over its 3D domain (and over time).

DOI: 10.2312/vmv.20141274

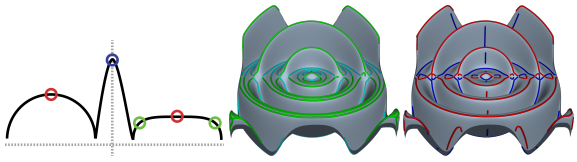

(a) Crease Points (b) Crease Lines

Figure 1: In (a) maximal crease points are shown for height (red), curvature (green) and both (purple). In (b) curvature-based crests (green) and valleys (cyan) on the left and height-based crests (red) and valleys (blue) on the right. Notice for a surface, creases need only be extremal in the direction of curvature.

We use an innovative data analysis and visualization method that leverages so-called crease surfaces [KTW06]. Creases are generalized local extrema defined for a function over a given domain. In the case of a curve defined by a single-valued function, creases can be defined as extrema in function value, curvature or both as illustrated in Fig. 1a. Surface creases, however, are defined as the set of points that are locally extremal in at least a single direction. This generalization of local extrema is represented by sets of crease lines which represent the crests and valleys of the surface, Fig. 1b. As the definition is applied to the 3D case, the connected crease points define surfaces, as shown in Fig. 2. The focus of research on creases in the 3D domain has been primarily on efficiently visualizing or extracting the crease surfaces using the height-ridge definition [EGM*94], which describes function-value-based crease surfaces.

We extend this previous work by suggesting a new and complementary definition for crease surfaces, motivated by well-established methodologies in the image-space [EGM*94] and graphics [OBS04] communities. Using this definition we can identify not only the function-value-based crease surfaces (height creases), but crease surfaces which are locally extremal in curvature (see Fig. 2). These curvature creases represent those areas in the volume where the shape of the underlying function exhibits extremal behavior. We show that for wave propagation, the curvature-based definition more completely and accurately represents the structure of individual wave fronts.

2. Related Work

Eberly et al. introduced the concept of ridges in image analysis [EGM*94]. This work is the basis for the most common definitions of creases or ridges. Lindeberg showed the importance of scale in ridge based feature selection [Lin96]. Kindlmann et al. more recently presented a way to accurately sample crease structure using a particle system in the 4D scale-space [KSJESW09]. Thirion defined a graph structure using extremal points and lines of curvature for medical surfaces [Thi96]. Both Ohtake et al. [OBS04] and later

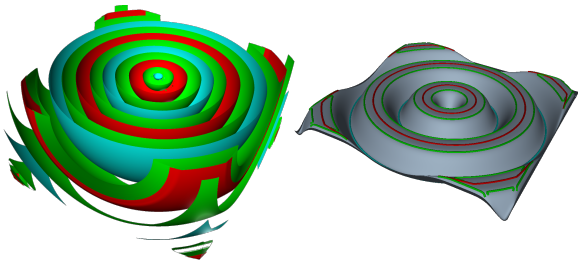

Figure 2: The crease surfaces for a sinusoidal function defined in the 3D domain is shown on the left. The maximal crease surfaces are shown for curvature-based creases (green) and height-based creases (red). The minimal crease surfaces (cyan) are equivalent under both the curvature and height definition. For context, we show a 2D slice from the volume.

Yoshizawa et al. [YBYS08] define ridges and valleys using curvature for triangulated surfaces. Our definition is a basic extension of this work for 3-manifolds. More recently, other definitions for crease like structures have been introduced for surfaces including the work on demarcating curves by Kolomenkin et al, which emphasize inflection points as zero crossings in the curvature field, [KST08]. Most recently, Norgard and Bermer presented a ridge-based graph structure using jacobi sets on height maps [NB13].

Crease surface visualization of volumetric data is an active area of ongoing research. Schultz et al. describe the topological properties of crease surfaces and how to extract them exactly [STS10]. Tricoche, Kindlmann, and Westin have perhaps been the most active in using crease surfaces for tensor field representing diffusion MRI data [KTW06], [TKW08]. Barakat interactively visualize and extract creases by effectively utilizing massively parallel GPUs: [BT10], [BAT11]. We use a similar implementation to [BT10] to enable interactive evaluation of crease surfaces. Obermaier et al [OMD*12] have shown the height-based valley creases are useful in visualizing low frequency sound waves. Our method captures a different yet related set of features which is able to more completely capture the wavefronts in more general settings.

Curvature has been used frequently in volume visualization. Armande et al. use extrema in the maximum and medium curvature of 3-manifolds to define crest lines or thin nets in volumetric data in order to extract blood vessels [AMM96]. Curvature has also been used to emphasize visualization on extracted surfaces in the volume [KWTM03].

In the seismology domain, Roberts defined semantics for curvature attributes including principal curvatures [Rob01]. Chopra and Marfurt expanded upon these to explore faults and fractures in volumetric datasets [ADM06]. Several case studies further validated these curvature semantics and their correlation with fault and fracture regions in seismic

datasets [SS03]. These rely mostly on 2D curvature and multi-spectral methods and have not been expanded to include higher order curvature attributes for scalar volumes.

3. Motivation

Our primary motivation is to define an intuitive and meaningful set of features for visualizing wave phenomena. We collaborated closely with domain scientists to describe the criteria needed for these features including: being representative of a waves structure, showing the relative intensity of the wave, and accurately capturing topological and shape changes due to interactions with the control structure (the propagation medium). However, it is also important that these fiduciary objects are not merely a visual aid but rather a true and objective measure of change with physical meaning.

Curvature-based crease surfaces best fit all of these requirements. Curvature has been long used to emphasize details in a wide variety of domains and has been used to highlight features, creases and regions of interest. Furthermore, various notions of energy are often directly related to second-degree derivative behavior of a function. The curvature of a hyper-surface itself is also directly related to second-order behavior of the function it's defined over. Curvature-based creases are local extremal behavior in curvature and can therefore provide meaningful insight into locally extremal energy behavior. In the case of volumetric wave systems, these crease surfaces correspond to physical wave fronts, whose shape, topology and motion are indicative of the wave field as a whole. Thus curvature-based crease surfaces are an ideal tool for the visualization of synthetic wave propagation data in the volumetric domain.

An obvious question is why use curvature creases, when the classic height-based definition often produces similar and sometimes equivalent sets of surfaces. Height ridges and valleys, in theory, should correspond well to the apex and troughs of wave fields, and in many cases they do. However, as wave fronts interfere with each other and interact with the control structure, complex wave forms result which are better defined by our curvature-based variant. This is especially true when the "shape" of the wave front begins to flatten out. Height-based creases are ill defined as the function plateaus, however curvature creases are well-defined at the edges of these plateaus. Our framework allows the user to easily switch or combine the different type of crease surfaces, however we will show that most often our curvature-based definition provides the most accurate and complete representation of the waves structure, Fig. 4.

4. Formal Definition of Crease Surfaces

Our method is grounded in differential geometry and uses the definition of principal curvature of a hyper-surface. Our definition for crease surfaces is a direct extension of the analogous work done for images [EGM*94] and triangulated surfaces [OBS04]. We define both the maximal and minimal crease surfaces (crests and valleys), which are mathematically dual to each other with respect to the orientation of the function-value axis. For completeness we define both curvature and height creases.

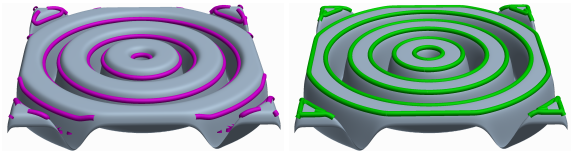

Figure 3: In the case of curvature-based creases, the Hessian-based definition (left) produces incorrect creases, while our method (right) produces the correct, expected crease lines. While the eigenvectors for the Hessian and (1) are equivalent, their eigenvalues are not.

4.1. Background: Principal Curvature

We calculate the principal curvatures and directions for the parametric hyper-surface $\mathcal{H}$ approximated by the graph $\mathcal{G} = (x, y, z, f(x, y, z))$ where f is a scalar field defined over the volumetric domain, f_x is the partial derivative of f in the x-direction and f_{xy} is the mixed partial derivative in the x and y-direction. The principal curvatures and directions of $\mathcal{H}$ are the eigenvalues and eigenvectors of the shape operator defined by the Gauss-Weingarten map [DC76] for the trivariate case [Ham94]. Note this is the combination of the first and second fundamental form from differential geometry.

$$A = \frac{1}{l}\begin{bmatrix} f_{xx} & f_{xy} & f_{xz} \\ f_{xy} & f_{yy} & f_{yz} \\ f_{xz} & f_{yz} & f_{zz} \end{bmatrix}\begin{bmatrix} 1+f_x^2 & f_x \cdot f_y & f_x \cdot f_z \\ f_x \cdot f_y & 1+f_y^2 & f_y \cdot f_z \\ f_x \cdot f_z & f_y \cdot f_z & 1+f_z^2 \end{bmatrix}^{-1} \quad (1)$$

where $l = \sqrt{1+f_x^2+f_y^2+f_z^2}$

The three real eigenvalues $\kappa_1, \kappa_2, \kappa_3$ and their eigenvectors τ_1, τ_2, τ_3 of A are the principal curvatures and directions ,respectively, of $\mathcal{H}$. In our application we use the maximum eigenvalue $\kappa_{max} = \mathbf{max}(\kappa_1, \kappa_2, \kappa_3)$ with its associated eigenvector τ_{max} and the minimum eigenvalue $\kappa_{min} = \mathbf{min}(\kappa_1, \kappa_2, \kappa_3)$ with its eigenvector τ_{min}. It must be noted that (1) is sometimes also presented as $-A$ in the literature. We chose not to negate the matrix A so that convex regions of the surface corresponded to κ_{min} and concave regions correspond to κ_{max}. Our motivation for this change was to more closely align our definition of crease-surfaces with the classic height-ridge definition, and avoid confusion.

4.2. Curvature Crease Surfaces

The crease surfaces with respect to curvature are defined by the set of all points $\mathbf{x}_i = (x_i, y_i, z_i)$ that are locally maximal

in the absolute value of principal curvature in the direction of curvature. This implies that directional derivative $\mathcal{E}(\mathbf{x}_i) = D_\tau\kappa(\mathbf{x}_i) = 0$. For maximal (crest) surfaces, $\mathcal{H}$ must be either locally convex or locally hyperbolic while $|\kappa_{min}| > \kappa_{max}$ at $\mathbf{x}_i$. This condition ensures that points in a saddle are correctly classified as maximal or minimal features based on the most dominant curvature term at that point. The valley surfaces are dual to the crest surface. More formally the crest (2) and valley surfaces (3) for curvature-based creases are defined by the following conditions:

$$\mathcal{E}_{min} = \frac{\partial \kappa_{min}}{\partial \tau_{min}} = 0 \quad \frac{\partial \mathcal{E}_{min}}{\partial \tau_{min}} > 0 \quad |\kappa_{min}| >= \kappa_{max} > 0 \quad (2)$$

$$\mathcal{E}_{max} = \frac{\partial \kappa_{max}}{\partial \tau_{max}} = 0 \quad \frac{\partial \mathcal{E}_{max}}{\partial \tau_{max}} < 0 \quad \kappa_{max} >= |\kappa_{min}| > 0 \quad (3)$$

It should be noted that due to the second term in (2,3), $D_\tau\mathcal{E}$, the above definitions require that f be a $\mathbf{C}^4$-continuous function. However, the directional derivative of curvature is simply a second derivative test, and it is therefore only important that one can determine its sign. We address the problem of smoothing the data and reducing noise in Section 5.1.

4.3. Height Crease Surfaces

While, to our knowledge, we are the first to use curvature values to define crease surfaces in the 3D domain, height-based creases that are extrema in function value, have become a popular tool for data visualization. For completeness we describe a slightly modified but equivalent definition discussed in earlier work for height-based crest (4) and valley (5) surfaces:

$$\nabla f \cdot \tau_{min} = 0 \quad |\kappa_{min}| >= \kappa_{max} > 0 \quad (4)$$

$$\nabla f \cdot \tau_{max} = 0 \quad \kappa_{max} >= |\kappa_{min}| > 0 \quad (5)$$

The only difference between our definition and the classic is that we use eigenvectors of (1) while other methods use the eigenvectors of the Hessian matrix. The matrix A and the Hessian have the same eigenvectors, see the discussion of the Gauss-Weingarten map and second fundamental form for surfaces of the type $(x, y, f(x, y))$ in [DC76], and we only use the eigenvectors of (1) and not the eigenvalues. Thus (4,5) are equivalent to the classic height-ridge definition.

4.4. Comparison

The feature sets described by curvature and height-based creases are often similar but represent different properties of the underlying function. Curvature-based creases represent abrupt changes in the normal of a surface. This often occurs at extremal regions of functional value, where height-based creases are defined, but not always. Curvature creases are not well-defined when curvature is constant while height-based creases are not well-defined when a function plateaus. Areas of locally constant curvature occur rarely in wave fields and

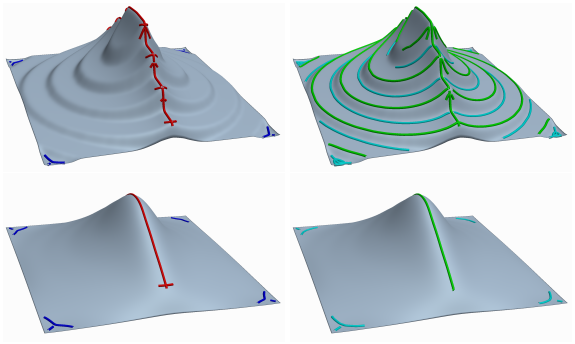

Figure 4: Top row: An analytically defined function with step-like plateaus is shown. Even with a moderate amount of smoothing, the height-based creases (left) cannot capture the plateau regions accurately, while the curvature-based creases (right) capture the structure. Bottom row: We smooth the function, until the height and curvature creases are the same. For wave fields, this level of smoothing removes valuable information regarding wave front changes.

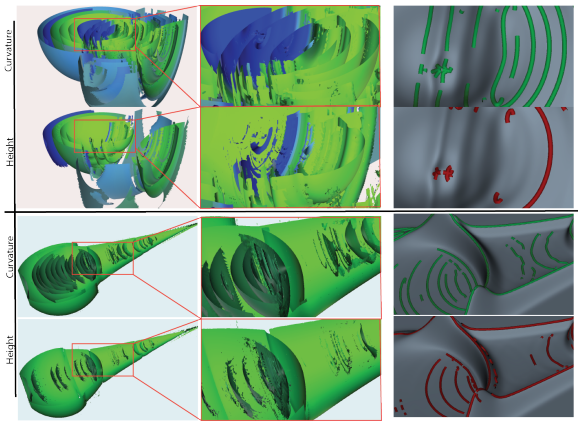

Figure 5: We compare and contrast the crest surfaces of curvature and height-based creases with color maps indicating negative (blue), and positive (green) pressure intensity. The curvature-based creases accurately represent the topology of the wave field, as highlighted in the center column. From a 2D slice, we can see the surface is similar to slanted steps which height-based creases are unable to accurately represent. These data sets are taken from an acoustic wave simulation. Two movies are attached showing the height and curvature-based crease surfaces in time for the bottom data set.

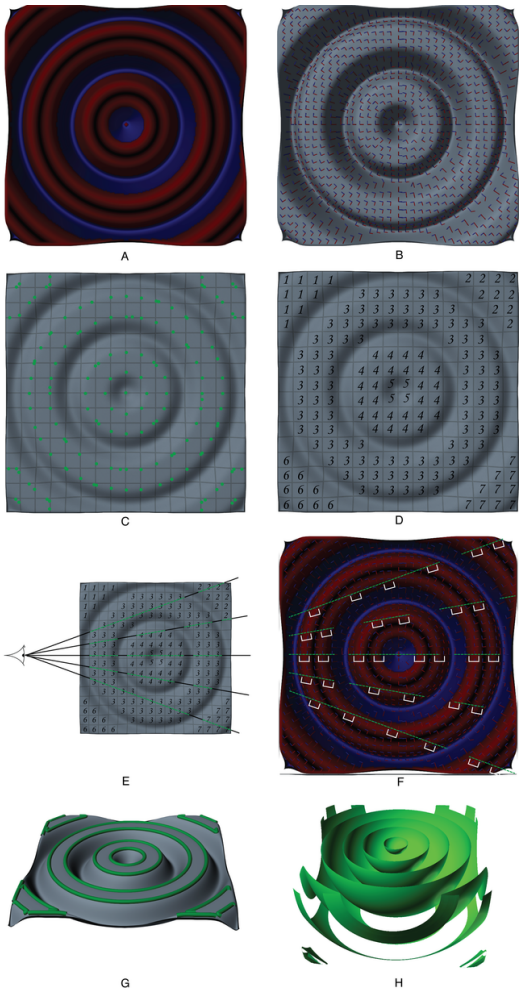

Figure 6: Our visualization algorithm uses adaptive ray casting to intersect crease surfaces using an interval-based bisection approach.

are easily dealt with by smoothing the field. Plateaus, however, can occur as wave fronts merge and as they reflect off medium boundaries, see Fig. 4. While in some cases smoothing can be applied until these plateaus disappear, this comes at the cost of losing significant information describing wave field changes, see Fig. 5. Both definitions are sensitive to noise and require applications where smoothing is appropriate. In practice we can greatly reduce the sensitivity to noise of curvature-based creases in wave front extraction to nearly the same qualitative levels as height-based creases. We use the eigenvectors of (1) instead of the equivalent eigenvectors for the Hessian when evaluating height creases out of convenience, however for curvature-based creases we must use (1) and not the Hessian to achieve correct results, see Fig. 3

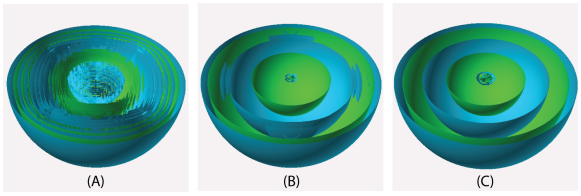

Figure 7: Varying levels of Gaussian smoothing are applied to a pressure wave propagating in a homogeneous medium: (A) $\sigma = 1.0$, (B) $\sigma = 2.0$, (C) $\sigma = 3.0$. In this example, we are able to completely remove all noise, and produce the correct surfaces corresponding to the wave fronts of interest.

5. Visualization Algorithm

Our visualization algorithm is based on performing GPU accelerated ray-casting through the volume and using an interval test to intersect rays with surfaces. Fig. 6 provides the details for visualizing creases. It is important to note that we were not the first to use this idea, [BT10] use a similar algorithm and structure to visualize creases, and [SN10] use a similar method to intersect implicit surfaces. We feel this is the most intuitive and obvious way to ray cast surfaces interactively on the GPU and include details to aid others in their implementation.

One major difference between our algorithm is the ability to do size based selection and filtering of crease surfaces based on the connected components defined by the coarse distance field we define in Fig. 6.

We first precompute principal curvature values for the volume, kmax and kmin, defining the magnitude and direction vector, Fig-6(A,B). We create a coarse distance field (CDF) for each set of crease surfaces, height/curvature and crest/valley, by finding edge intersections on a uniform rectilinear grid of a 3D domain, (C). We calculate the connected components of cells which contain a crease surface, as they have surface intersections on one or more of the cell boundaries. All crease surfaces in connecting cells are treated as if they are connected, and the number of connected cells represents the relative size of contained surfaces, thus the resolution of the CDF grid greatly impacts the effectiveness of these connected components. We mark each cell by an id corresponding to there connected component or by a null value (D). We then mark each null cell whose neighbor contains a surface. When ray casting, the CDF allows us to adaptively set the ray step size larger, when we are not in or adjacent to a cell containing a crease surface. We can also filter out smaller suffices, by flagging those cells. To intersect the surfaces, we use an interval test based on bisection (E,F).

5.1. Calculating Curvature Creases and Reducing Noise

The direct calculation of curvature-based creases (2,3) requires **class C^4** continuity, which implies that they are

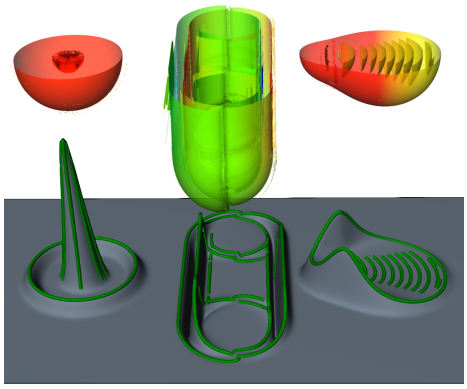

Figure 8: We show the curvature crease crests corresponding to the individual wave fronts propagating from three independent sources.

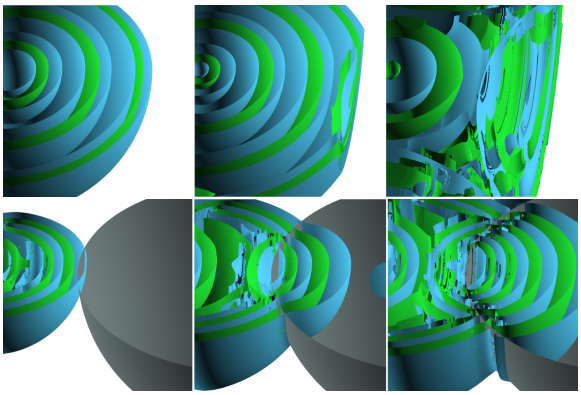

Figure 9: Curvature-based crease surfaces visualizing pressure (acoustic) waves, highlighting reflection, refraction and interference. Top: crest (green) and valley (cyan) creases we show the reflection off a boundary layer (not shown), and the resulting interference pattern as the reflected wave intersects. Bottom: We show the wave fronts reflecting off and refracting through the dense outer core of the Preliminary Reference Earth Model (PREM).

extremely sensitive to high frequency noise. However, we circumvent noise sensitivity by only calculating the sign for $\mathcal{E}$ to do an interval test. Additionally the sign of $\frac{\partial \mathcal{E}}{\partial \tau}$ is only needed as the second derivative (of curvature) test. In practice, noise affects curvature-based creases only slightly worse than height-based creases.
We use finite differencing to calculate the derivatives for (1). Also, we use decomposed trilinear interpolation to estimate κ and τ, such that τ is locally oriented in each step of the interpolation. This is necessary as eigenvectors are not globally orientable. We estimate the directional derivatives for (2,3) as follows:

$$\mathcal{E}_* \approx \frac{\kappa_*|_{p+\tau_*} - \kappa_*|_{p-\tau_*}}{2}, \quad \frac{\partial \mathcal{E}_*}{\partial \tau_*} \approx \kappa_*|_{p+\tau_*} - \kappa_*|_p + \kappa_*|_{p-\tau_*}$$

We are only interested in the sign of $\mathcal{E}$ and $\frac{\partial \mathcal{E}}{\partial \tau}$ so approximation is appropriate for our use case.

To reduce the effect of noise further, we apply a user-controlled Gaussian smoothing. Lindeberg gives a method for automatic scale space selection in [Lin96], which has also been applied to crease surfaces [BT10]. In our framework, the user chooses a scaling because they have a good understanding of the frequency domain for features and noise. Finally, we define a mapping of crease surfaces with connected components, Fig. 6(D), to threshold the surfaces by feature size.

6. Application

We present the efficacy of our method in extracting wave fronts and visualizing wave phenomena. We use examples from pressure (acoustic) waves, and the TeraShake 2.1 seismic simulation from a hypothetical magnitude 7.7 earthquake.

6.1. Evaluation

We tested the accuracy of our method in extracting wave fronts by qualitatively comparing crease surfaces with multiple slices taken from each data set. Fig. 8 shows our ability to accurately visualize the wave fronts resulting from point, planar and moving sources using curvature-based crease surfaces. Fig. 4 shows two cases where curvature-based creases accurately represents the structure of the wave field.

Several relevant wave-based phenomena are intuitively shown using our method. The type of wave, properties of the medium and material density all affect how wave fronts reflect , refract or both through the medium. We highlight our ability to capture this behavior in Fig. 9. When wave fronts intersect with each other an interference occurs that can cause significant changes in the shape and topology of t8he wave fronts. One well known example is the Doppler effect caused by a moving source. In Fig. 4, the wave fronts accurately depict this effect, and show the topology change which occurs when the acoustic source (in this case) accelerates past the sound-barrier.

6.2. Preliminary Reference Earth Model

The Preliminary Reference Earth Model, PREM, represents the interior of the earth as a solid sphere of concentric shells with varying density. While it is not an accurate representation of the earth, it does represent a complex and pseudo-realistic medium for waves to travel through. In Fig. 10, we show the curvature-based crest surfaces of an acoustic wave originating at two independent point sources within the PREM. We visualize the changes in waves structure

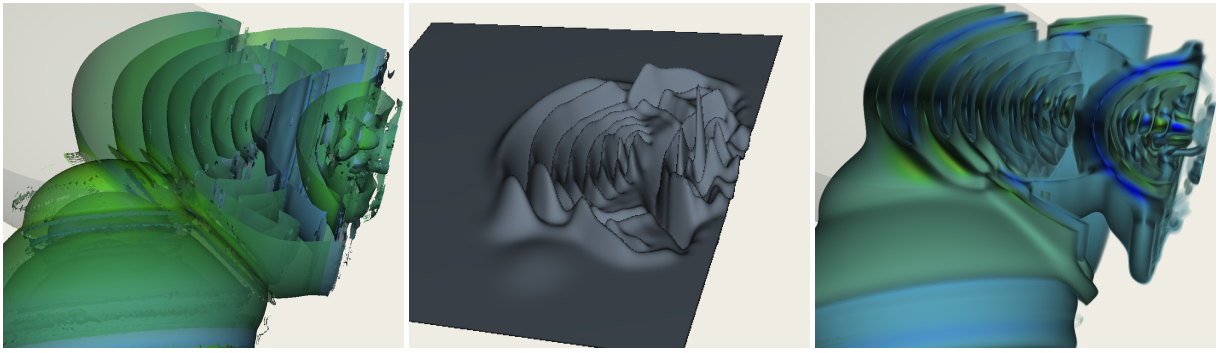

Figure 10: We show curvature based creases, a slice, and a volume rendering of waves in the Preliminary Earth Model. The crease surfaces best and most completely represent the wave fronts revealing the relevant scientific phenomena.

as it reflects and refracts off the outer core (grey sphere) which is much greater density than the mantle. The interference occurs between wave fronts as they meet from different sources. As the wave hits the core, it reflects and refracts, traveling faster in the denser medium, stretching the center of the wave front. Eventually, this combination causes the wave front to bifurcate. This change in topology is expected and is visually represented best by our crest surfaces. We attached a movie of the curvature-based crease surfaces for this data set which show the surfaces evolving over time.

In Fig. 10, the 2D plane shows features, but gives no indication of volumetric changes and thus hides the reason for interference between wave fronts. We chose a transfer function to best represent the wave fronts in the volume rendering. This would have to be updated constantly as time progressed, and still does not give the fidelity needed to show evolution of individual wave fronts.

6.3. Terashake 2.1

The dataset used in Fig. 11 is the product of a simulation of a hypothetical magnitude 7.7 earthquake on the southern San Andreas fault (California, USA), TeraShake2. To improve assessments of the seismic hazard of populated regions, geophysicists have been simulating the fault rupture and the resultant shaking, as the seismic waves propagate through the Earth's crust (e.g. [COC*09]). These simulations involve computing the progress of elastic seismic waves through subsurface geologic structure. Visualization of the evolving field is critically important for gaining insight [CCC*07]. Visualization enables the user to observe reflections and refractions due to the subsurface structure, and reveals which structures are responsible for focusing and directing the waves, seen in Fig. 11.

7. Limitations

Our method is not always able to accurately resolve the edges of crease surfaces, especially when they are very thin and degenerate into crease surfaces, or when a crease surface bifurcates. Our size filtering method is not perfect, and depends greatly on the size of the course distance field used. We have difficulty handling some types of high-frequency noise, however this is no worse for curvature creases as it is for height. All of these issues can be solved by extracting the surfaces, investigating better methods for smoothing, and applying thresholds on the extracted surfaces.

8. Conclusion

We present a new analytical definition for visualizing curvature-based crease surfaces that intuitively represent wave fronts in wave propagation data. These crease surfaces act as fiduciary objects that allow the user to understand the structure and motion of a wave field as it changes over time. We have shown the effectiveness of this method for visualizing the structure and topology of wave fronts and representing reflection, refraction, and interference. In the future, we will investigate curvature-based crease surfaces in other applications. We will continue to investigate the differences between creases defined by height and curvature and their topological properties. We are also interested in better understanding the effectiveness of different smoothing techniques, scale space optimization, and thresholding parameters on minimizing noise in our visualization.

Aknowledgments

This work was supported in part by the "Los Alamos National Laboratory - UC Davis Institute of Next-generation Visualization and Analysis (INGVA)," a collaborative educational and research training effort performed jointly by Los Alamos National Laboratory (LANL) and UC Davis. The authors especially thank the members of the LANL Data Science at Scale Group, the UC Davis W.M. Keck Foundation Center for Active Visualization in the Earth Sciences (KeckCAVES), and the UC Davis Institute for Data Analysis and Visualization (IDAV).

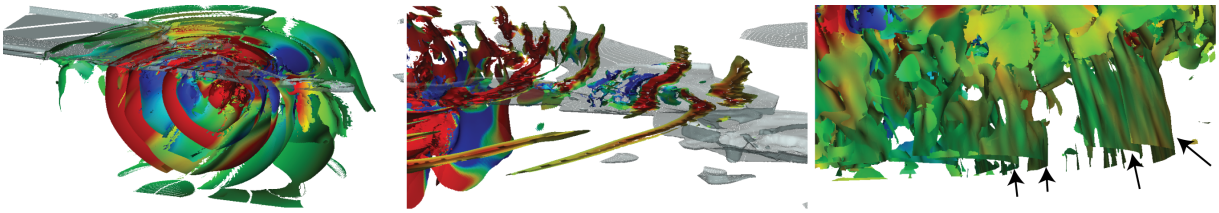

Figure 11: The TeraShake 2.1 data set is a large-scale earth quake simulation of a 7.7 earthquake on the southern San Andreas fault traveling over the Los Angeles sedimentary basins (grey). (A) shows the wave as it propagates along the fault rupture. We clip the volume along the fault to show individual wave fronts. In (B), wave fronts are focused and directed through a sedimentary basin. We are able to interactively filter the wave fronts so that only the ones of interest are shown. Finally in (C), we highlight wave fronts which have reflected off dense materials in the control structure and are traveling in the opposite direction of the primary wave. To our knowledge these fronts have not been shown using any other methods of visualization.

References

[ADM06] AL-DOSSARY S., MARFURT K. J.: 3D volumetric multispectral estimates of reflector curvature and rotation. *Geophysics 71*, 5 (SEP-OCT 2006), P41–P51. 2

[AMM96] ARMANDE N., MONTESINOS P., MONGA O.: A 3D thin nets extraction method for medical imaging. 642–646 vol.1. 2

[BAT11] BARAKAT S., ANDRYSCO N., TRICOCHE X.: Fast Extraction of High-quality Crease Surfaces for Visual Analysis. *Computer Graphics Forum 30*, 3 (2011), 961–970. 2

[BT10] BARAKAT S., TRICOCHE X.: An image-based approach to interactive crease extraction and rendering. *Procedia Computer Science* (2010). 2, 4, 6

[CCC*07] CHOURASIA A., CUTCHIN S., CUI Y., MOORE R. W., OLSEN K., DAY S. M., MINSTER J. B., MAECHLING P., JORDAN T. H.: Visual Insights into High-Resolution Earthquake Simulations. *Computer Graphics and Applications, IEEE 27*, 5 (2007), 28–34. 7

[COC*09] CUI Y., OLSEN K., CHOURASIA A., MOORE R., MAECHLING P., JORDAN T.: The TeraShake Computational Platform for Large-Scale Earthquake Simulations. In *Advances in Geocomputing*. Springer Berlin Heidelberg, Jan. 2009, pp. 229–277. 7

[DC76] DO-CARMO M. P.: *Differential Geometry of Curves and Surfaces*, first ed. Prentice Hall, Feb. 1976. 3, 4

[EGM*94] EBERLY D., GARDNER R., MORSE B., PIZER S., SCHARLACH C.: Ridges for image analysis. *J. Math. Imaging Vis. 4*, 4 (1994), 353–373. 2, 3

[Ham94] HAMANN B.: Curvature approximation of 3d manifolds in 4d space. *Comput. Aided Geom. Des. 11* (December 1994), 621–632. 3

[KSJESW09] KINDLMANN G., SAN JOSÉ ESTÉPAR R., SMITH S. M., WESTIN C.-F.: Sampling and visualizing creases with scale-space particles. *IEEE Transactions on Visualization and Computer Graphics 15*, 6 (2009), 1415–1424. 2

[KST08] KOLOMENKIN M., SHIMSHONI I., TAL A.: Demarcating curves for shape illustration. *ACM Transactions on Graphics* (2008). 2

[KTW06] KINDLMANN G., TRICOCHE X., WESTIN C.-F.: Anisotropy Creases Delineate White Matter Structure in Diffusion Tensor MRI. In *Medical Image Computing and Computer-Assisted Intervention – MICCAI 2006*. Springer Berlin Heidelberg, Jan. 2006, pp. 126–133. 2

[KWTM03] KINDLMANN G., WHITAKER R., TASDIZEN T., MOLLER T.: Curvature-based transfer functions for direct volume rendering: Methods and applications. In *Proceedings of the 14th IEEE Visualization 2003 (VIS'03)* (Washington, DC, USA, 2003), VIS '03, IEEE Computer Society, pp. 67–. 2

[Lin96] LINDEBERG T.: Edge detection and ridge detection with automatic scale selection. *International Journal of Computer Vision 30* (1996), 465–470. 2, 6

[NB13] NORGARD G., BREMER P.-T.: Ridge–Valley graphs: Combinatorial ridge detection using Jacobi sets. *Computer Aided Geometric Design 30*, 6 (July 2013), 597–608. 2

[OBS04] OHTAKE Y., BELYAEV A., SEIDEL H. P.: Ridge-valley lines on meshes via implicit surface fitting. *ACM Transactions on Graphics (TOG)* (2004). 2, 3

[OMD*12] OBERMAIER H., MOHRING J., DEINES E., HERING-BERTRAM M., HAGEN H.: On Mesh-Free Valley Surface Extraction with Application to Low Frequency Sound Simulation. *IEEE Transactions on Visualization and Computer Graphics 18*, 2 (Feb. 2012), 270–282. 2

[Rob01] ROBERTS A.: Curvature attributes and their application to 3D interpreted horizons. *First Break 19*, 2 (2001), 85–100. 2

[SN10] SINGH J. M., NARAYANAN P. J.: Real-Time Ray Tracing of Implicit Surfaces on the GPU. *Visualization and Computer Graphics, IEEE Transactions on 16*, 2 (2010), 261–272. 4

[SS03] SIGISMONDI M. E., SOLDO J. C.: Curvature attributes and seismic interpretation: Case studies from Argentina basins. *The Leading Edge 22*, 11 (2003), 1122–1126. 3

[STS10] SCHULTZ T., THEISEL H., SEIDEL H.-P.: Crease Surfaces: From Theory to Extraction and Application to Diffusion Tensor MRI. *IEEE Transactions on Visualization and Computer Graphics 16*, 1 (Jan. 2010), 109–119. 2

[Thi96] THIRION J.-P.: The extremal mesh and the understanding of 3D surfaces. *International Journal of Computer Vision 19*, 2 (Aug. 1996), 115–128. 2

[TKW08] TRICOCHE X., KINDLMANN G., WESTIN C.-F.: Invariant crease lines for topological and structural analysis of tensor fields. *Visualization and Computer Graphics, IEEE Transactions on 14*, 6 (Nov. 2008), 1627 –1634. 2

[YBYS08] YOSHIZAWA S., BELYAEV A., YOKOTA H., SEIDEL H.-P.: Fast, robust, and faithful methods for detecting crest lines on meshes. *Computer Aided Geometric Design 25*, 8 (Nov. 2008), 545–560. 2